



# Symmetric tangled Platonic polyhedra

Stephen T. Hyde<sup>a,1,2</sup> and Myfanwy E. Evans<sup>b,1</sup>

<sup>a</sup>School of Chemistry, The University of Sydney, Sydney, New South Wales 2006, Australia; and <sup>b</sup>Institute for Mathematics, University of Potsdam, 14476 Potsdam, Germany

Edited by James Sethian, Department of Mathematics, University of California, Berkeley, CA; received June 3, 2021; accepted October 25, 2021

**Conventional embeddings of the edge-graphs of Platonic polyhedra,  $\{f, z\}$ , where  $f, z$  denote the number of edges in each face and the edge-valence at each vertex, respectively, are untangled in that they can be placed on a sphere ( $S^2$ ) such that distinct edges do not intersect, analogous to unknotted loops, which allow crossing-free drawings of  $S^1$  on the sphere. The most symmetric (flag-transitive) realizations of those polyhedral graphs are those of the classical Platonic polyhedra, whose symmetries are  $*2fz$ , according to Conway's two-dimensional (2D) orbifold notation (equivalent to Schönflies symbols  $I_h$ ,  $O_h$ , and  $T_d$ ). Tangled Platonic  $\{f, z\}$  polyhedra—which cannot lie on the sphere without edge-crossings—are constructed as windings of helices with three, five, seven, ... strands on multigenus surfaces formed by tubifying the edges of conventional Platonic polyhedra, have (chiral) symmetries  $2fz$  ( $I$ ,  $O$ , and  $T$ ), whose vertices, edges, and faces are symmetrically identical, realized with two flags. The analysis extends to the " $\theta_z$ " polyhedra,  $\{2, z\}$ . The vertices of these symmetric tangled polyhedra overlap with those of the Platonic polyhedra; however, their helicity requires curvilinear (or kinked) edges in all but one case. We show that these  $2fz$  polyhedral tangles are maximally symmetric; more symmetric embeddings are necessarily untangled. On one hand, their topologies are very constrained: They are either self-entangled graphs (analogous to knots) or mutually catenated entangled compound polyhedra (analogous to links). On the other hand, an endless variety of entanglements can be realized for each topology. Simpler examples resemble patterns observed in synthetic organometallic materials and clathrin coats in vivo.**

regular polyhedra | compound polyhedra | helicates | metal-organic frameworks | clathrin

Two-dimensional topology, graph theory, and non-Euclidean geometry offer a useful view of the rich universe of chemical structures. In this paper, we combine Platonic geometry and two-dimensional topology to derive theoretical families of "tangled" or "catenated" polyhedra, whose faces are threaded by edges. (We will clarify our nomenclature later on.) The resulting structures are worth knowing for their own sake, since they are the most symmetric entanglements of the regular (Platonic) polyhedra in three-dimensional space, with symmetrically equivalent faces, edges, and vertices. They are also promising candidates for (supra)molecular assemblies. For example, tangled symmetric structures are a feature of finite metal-organic molecules (1–5) and infinite catenated inorganic compounds, coordination polymers, covalent organic frameworks (COFs), and metal-organic frameworks (MOFs) (6–12).

The phenomenon of entanglement is central to the mathematical field of knot theory (13). Equivalent tangled nets are "isotopic" and interchangeable by any distortion of the net edges and vertices as long as edges don't pass through each other. Tangling is therefore a structural phenomenon that lies between geometrically congruent structures, which allow rigid-body rotations or translations only, and topologically equivalent (homeomorphic) structures, which can be interchanged by arbitrary distortions, including "phantom moves" of edges through each other. In common with modern understanding of polyhedra as combinatorial structures (14), we describe polyhedra via the net of edges and vertices, allowing faces to self-intersect. However,

we do not insist that edges follow shortest paths between vertices, allowing edges to tangle. For example, tangled cubes share the topology of the conventional Platonic cube, but many different "isotopes" are possible, whose rings of four edges—bounding the cube "faces"—are threaded by edges in different ways (some examples can be found in ref. 15). The occurrence of tangled two- and three-periodic nets at the molecular scale in synthetic chemical materials, particularly MOFs, has led to a number of fundamental studies of tangles of infinite periodic nets (10, 16–19). In contrast, surprisingly little is known about allowed symmetries of finite nets, with the exception of the "trivial" (untangled) symmetric (e.g., Platonic and Archimedean) polyhedra and studies of symmetric embeddings of knots and links (20–22). Graph topologies of the five Platonic polyhedral nets are given by their Schläfli symbols,  $\{f, z\}$ , where  $f$  describes the number of edges per face and  $z$  the number of faces per vertex ( $z$ ), including  $\{3, 3\}$  (tetrahedron),  $\{3, 4\}$  (octahedron),  $\{4, 3\}$  (cube),  $\{3, 5\}$  (icosahedron), and  $\{5, 3\}$  (dodecahedron). We describe the familiar regular embeddings of these nets, with straight edges, as (capitalized) "Platonic" embeddings and arbitrary embeddings of  $\{f, z\}$  nets as "platonic". The former are "flag-transitive" embeddings of  $\{f, z\}$  nets with symmetrically identical faces, edges, and vertices; their point-group symmetries are (for our purposes) most simply denoted by Conway's orbifold symbols  $*2fz$  (23). The orbifolds refer to the symmetries of spherical embeddings of the Platonic polyhedra, formed by blowing the polyhedra into a ball, bounded by a sphere centered on the

## Significance

**Tangled tetrahedra, octahedra, cubes, icosahedra, and dodecahedra are generalizations of classical—untangled—Platonic polyhedra. Like the Platonic polyhedra, all vertices, edges, and faces are symmetrically equivalent. However, the edges of tangled polyhedra are curvilinear, or kinked, to allow entanglement, much like warps and wefts in woven fabrics. We construct the most symmetric entanglements of these polyhedra via assemblies of multistrand helices wound around edges of the conventional polyhedra; they are all necessarily chiral. The construction gives self-entangled chiral polyhedra and compound polyhedra containing catenated multiple tetrahedra or "generalized  $\theta$ -polyhedra." An unlimited variety of tangling is possible for any given topology. Related structures have been observed in synthetic materials and clathrin assemblies within cells.**

Author contributions: S.T.H. and M.E.E. designed research; S.T.H. and M.E.E. performed research; S.T.H. and M.E.E. analyzed data; and S.T.H. wrote the paper.

The authors declare no competing interest.

This article is a PNAS Direct Submission.

This open access article is distributed under [Creative Commons Attribution-NonCommercial-NoDerivatives License 4.0 \(CC BY-NC-ND\)](https://creativecommons.org/licenses/by-nc-nd/4.0/).

<sup>1</sup>S.T.H. and M.E.E. contributed equally to this work.

<sup>2</sup>To whom correspondence may be addressed. Email: [stephen.hyde@sydney.edu.au](mailto:stephen.hyde@sydney.edu.au).

This article contains supporting information online at <https://www.pnas.org/lookup/suppl/doi:10.1073/pnas.2110345118/-DCSupplemental>.

Published January 4, 2022.

polyhedron. The radius of that sphere can be adjusted so that all polyhedral vertices lie on its surface and edges form arcs of great circles joining those vertices. Conway symbols  $*2fz$  describe the asymmetric domain of those spherical Platonic polyhedra: spherical triangles bounded by geodesic mirror arcs (on great circles) subtending angles on the sphere of  $\frac{\pi}{2}$ ,  $\frac{\pi}{f}$ , and  $\frac{\pi}{z}$ . The geodesic edges coincide with the intersections of mirror planes of the Platonic polyhedron with the sphere, passing through face centers, vertices, and midedges, giving Schönflies point-group symbols,  $T_d$ ,  $O_h$ , and  $I_h$  (for  $\{3, 3\}$ ,  $\{4, 3\}$  or  $\{3, 4\}$ , and  $\{5, 3\}$  or  $\{3, 5\}$ , respectively) (24).

Graph topologies of the nets of platonic polyhedra are constrained by Euler's formula for polyhedra, which can be expressed as  $0 \leq (f - 2)(z - 2) < 4$ , where  $f$  and  $z$  are positive integers. That relation admits additional solutions, notably, the  $\{2, 3\}$  “ $\theta$ -polyhedron,” with a pair of three-valent vertices and three lens-shaped faces. That net can be embedded in space with symmetry  $*223$ , in which case its three edges describe curved meridians from pole to pole. More generally,  $\theta_z$ -polyhedra, with vertices at both poles joined by  $z$  meridians, are admissible solutions. For convenience, we include the  $\theta_z$ -polyhedra among platonic examples. All of these platonic  $\{f, z\}$  polyhedra can be embedded as “regular” (Platonic) polyhedra, with reflection symmetry  $*2fz$ .

The most symmetric “irregular” polyhedra are referred to as “chiral polytopes” in ref. 25. So-called chiral polytopes are almost, but not quite, regular: Like regular polyhedra, they have edge-, vertex-, and face-transitive embeddings. However, in contrast to regular cases which have a single flag, chiral polytopes have two distinct flags, each with separate orbits. Any flag of one type is necessarily adjacent to a flag of the other, and their union describes an asymmetric domain of the chiral embedding (25). (Three-dimensional chiral polytopes differ from better-known chiral polyhedra, such as the snub cube, although both are geometrically chiral.) Chiral polytopes, with straight edges, include either an infinite number of finite (skew) faces or a finite number of infinite (helical) faces (25). Here, we show that specific entanglements of  $\{f, z\}$  polyhedra, whose nets share the topologies of Platonic polyhedra, can be realized with symmetries  $2fz$ , which contain rotation axes only (Schönflies point-group symbols  $T$ ,  $O$ , and  $I$  for  $\{3, 3\}$ ,  $\{4, 3\}$  or  $\{3, 4\}$ , and  $\{5, 3\}$  or  $\{3, 5\}$ , respectively). The edge-net of a tangled platonic  $\{f, z\}$  polyhedron cannot be morphed into that of its untangled Platonic analog without phantom crossings, where edges pass through each other. Like chiral polytopes, these tangled polyhedra have just two flags; they are therefore the most symmetric nontrivial embeddings of entangled platonic graphs, whose trivial entanglements are the Platonic  $*2fz$  polyhedral embeddings.

Embeddings of Platonic  $\{f, z\}$  polyhedra with no crossed edges are possible on the sphere; their edges can therefore be traced in the plane without edge-crossings (e.g., via stereographic projection). These regular embeddings are classified as “untangled,” analogous to the trivial unknot, which can be drawn in the plane (or on the sphere) without edge-crossings. In contrast, like knots, planar drawings of tangled net embeddings contain edge-crossings, and crossing-free embeddings are possible only on higher-genus surfaces. Tangled embeddings of polyhedral nets  $\{f, z\}$  are less symmetric than their untangled, regular analogs. Earlier studies of tangled nets of the tetrahedron, octahedron, and cube, generated as reticulations of the relevant  $\{f, z\}$  nets on the torus, established that all such “toroidal polyhedra” are topologically chiral (26, 27), allowing a pair of distinct isotopes related to each other by a reflection. Further, those toroidal polyhedra are, without exception, rather asymmetric compared with their untangled embeddings. Their chirality ensures that they are devoid of reflections (so their orbifold symbols exclude the  $*$  character) and have multiple flags. The most symmetric toroidal tetrahedra, cubes, and octahedra can

be realized with orbifolds  $222 (D_2)$ ,  $422 (D_4)$ , and  $622 (D_6)$ , respectively (28), with six, six, and four distinct flags. Here, we show that the most symmetric  $\{f, z\}$  (nontrivially) tangled polyhedral nets can be embedded in space with chiral symmetry  $2fz$ , provided their edges are curved (or suitably kinked), so that they have just two flags, analogous to chiral polytopes. Since the most symmetric regular embeddings of polyhedral graphs  $\{f, z\}$ , with symmetry  $*2fz$ , are untangled, these  $2fz$  cases are the most symmetric possible embeddings of (nontrivial) polyhedral entanglements.

### Construction of $2fz$ Polyhedra

Less symmetric tangled toroidal polyhedra introduced above are analogous to torus knots, which are formed by winding a loop on the surface of a (genus-one) torus—a donut. Simpler torus knots are the trefoil knot and two-component Hopf link. These are conventionally labeled  $3_1$  and  $2_1^2$ , respectively, where label  $X_i^L$  indicates a knot (no superscript) or  $L$ -component link that can be drawn on the page with no fewer than  $X$  crossings, and  $i$  is an arbitrary index to distinguish different knots or links with minimal crossing number  $X$ . To form  $3_1$  and  $2_1^2$ , a pair of parallel strands is wound around the torus once, building what we call a “two-track railway” on the torus. That railway passes through a single twist box with two ports for each track, such that its entry and exit ports for each track are set by the (even or odd) parity of the number of half-twists,  $t$ . Within the switch box, the tracks wind around each other, giving a double-helix with  $t$  half-twists. The resulting knot depends on  $t$ :  $2_1^2$  and  $3_1$  form by setting  $t$  to two and three, respectively, and winding the two-track railway, denoted  $\frac{t}{2}$  on the torus, then removing the torus, leaving the railway embedded in three-space. We label these torus knots by their “railway labels,”  $\frac{2}{2}$  (Hopf) and  $\frac{3}{2}$  (trefoil). The constructions are shown in Fig. 1.

Since these railways are formed by double-helical windings around the torus, their embeddings are geometrically chiral, whose enantiomers have railways  $\frac{-2}{2}$  and  $\frac{-3}{2}$ , respectively. The  $\frac{-2}{2}$  railway can be deformed without phantom moves to give the same three-dimensional embedding as that of the  $\frac{2}{2}$  railway, so both  $\frac{-2}{2}$  and  $\frac{2}{2}$  form the same isotope, and the Hopf link is “topologically achiral.” It is, in fact, the sole topologically achiral knot or link among all  $\frac{\pm t}{2}$  railways (excluding the unknotted  $\frac{0}{2}$  and  $\frac{1}{2}$  railways). In contrast, the pair of geometrically enantiomeric railways  $\frac{-3}{2}$  and  $\frac{3}{2}$  are distinct isotopes, and the trefoil knot is topologically chiral, with enantiomers  $3_1^+$  and  $3_1^-$ . Higher-order helices, with  $n = 3, 4, \dots$  strands, can also be wound on the torus,

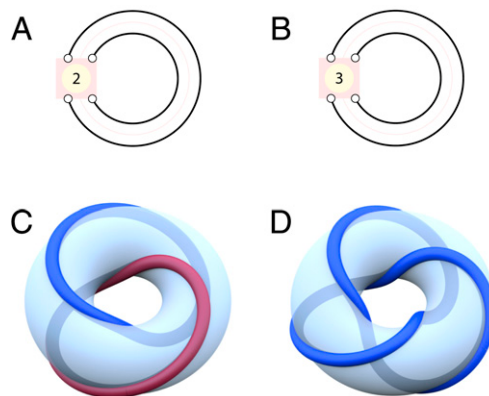


**Fig. 1.** (A and B) Schematic drawings of two-track railways lining the torus, characterized by a pair of parallel strands, interrupted by a single (pink) twist box, where the tracks experience two (A) and three (B) half-twists, forming  $\frac{2}{2}$  and  $\frac{3}{2}$  railways, respectively. The railways form tangles in three-dimensional space. (C and D) A Hopf link ( $2_1^2$ ; C) and a trefoil knot ( $3_1$ ; D).

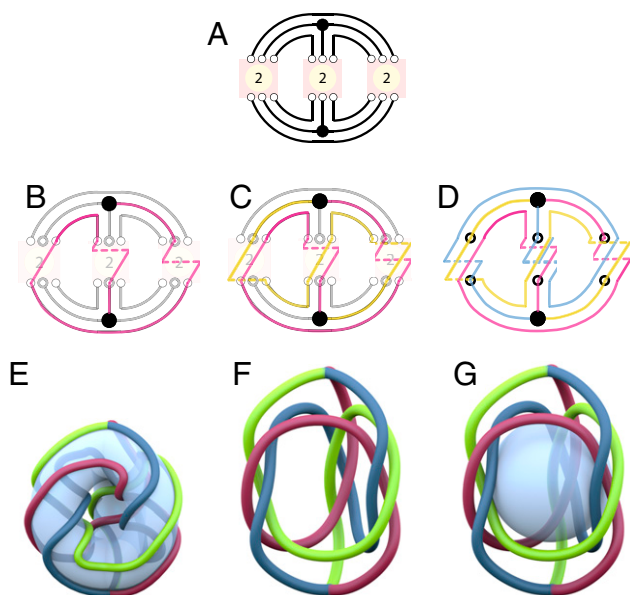


**Fig. 2.** Construction of the  $[\frac{2}{3}]_{\theta}^3$  tangled polyhedron. (A) Schematic planar cartoon of the winding, with three parallel strands running along each tubified edge of the  $\theta$ -graph, forming a triple-helix whose strands are twisted by  $\frac{4\pi}{3}$  along each tubule ( $t = 2$ ). (B–D) The trajectory of crimson, yellow, and blue tracks, twisted within each switch, building the vertex- and edge-transitive polyhedral tangle. (E) The three-track winding on the tubified  $\theta$ -polyhedron. The  $\theta$ -skeleton is embedded with maximal symmetry  $*223$ , giving a tangled polyhedron with symmetry  $223$ . (F) The resulting  $[\frac{2}{3}]_{\theta}^3$  tangle embedded in space, after removal of the bitorus. (G) Alternative view of the tangle, with a central opaque sphere as a visual aid.

forming  $n$ -track railways  $\frac{t}{n}$ , where each strand is twisted by  $\frac{2\pi t}{n}$  during a single traverse around the torus.

In contrast to torus knots and links, the tangled polyhedra we construct are realized by winding  $n$ -stranded helices on a “polytorus,” an oriented boundary-free surface, whose genus exceeds one. Polytori are formed from the edges of a symmetric skeleton, whose edges are those of a Platonic polyhedron  $\{f, z\}$ , or the “ $\theta$ ” polyhedra,  $\{2, z\}$ . Tubification of the skeleton (replacing its edges by tubules) results in the polytorus of genus  $g = \frac{2z+f(z-2)}{2z-f(z-2)}$ , whose symmetries are those of its underlying skeleton,  $*2fz$ . We construct symmetric polyhedral tangles as follows. Each tubule hosts the same  $n$ -strand helix, with equal twist  $t$ ,  $\frac{t}{n}$ , where  $n$  is odd ( $n = 2k + 1$ ). The central strand on each tubule runs between vertices of the polyhedral graph, whereas outer strands of adjacent tubules are joined, forming a helically wound graph, via a construction outlined in detail in the next paragraph. An infinite variety of polyhedral entanglements are generated by varying  $n$  and  $t$ , as well as the polyhedral skeleton. We label each tangled polyhedron  $[\frac{t}{2k+1}]_P^E$ , formed by winding a helix with  $2k + 1$  parallel strands and twist  $t$  around each tubule of the polytorus, whose skeleton is the edge-graph of the polyhedron  $P$  with  $E$  edges. Like the toroidal tangled polyhedra discussed above, the edges of these polytoroidal tangled polyhedra do not describe maps on their underlying surface since they do not bound  $z$ -disk-like faces. [Their universal covers are close-packed  $z$ -branched trees, embedded in the hyperbolic plane,  $\mathbb{H}^2$  (29).]

For example, a tangled polyhedron  $[\frac{2}{3}]_{\theta}^3$  is built by winding three tracks on a genus-2 bitorus, formed by tubifying the three-valent  $\theta$ -graph, building a bitorus of symmetry  $223$ , as shown in Fig. 2. A single edge is traced from a point on the tubified  $\theta$ -polyhedron corresponding to a vertex in the skeleton, along a tubule, and winds around each tubule, twisting by an angle of  $\frac{2\pi t}{n} = \frac{4\pi}{3}$  as it passes through each twist box. Fig. 2B reveals

that each edge of the tangle traverses all three tubules of the  $\theta$  bitorus: The crimson edge exits the upper vertex, then passes through the right-hand tubule, followed by the left-hand tubule and the central tubule, terminating at the lower vertex. The edge-topology of this three-track railway is that of the  $\theta$ -graph: a pair of three-valent vertices joined by three edges. However, it is not the same isotope as the usual (untangled)  $\theta$ -polyhedron, since its edges cannot be relaxed to form that untangled embedding without passing through themselves; it is therefore (nontrivially) tangled. In this case, its tangling is manifested by knotted loops. For example, the closed two-ring including crimson and yellow edges only in Fig. 2C forms a trefoil knot,  $3_1^+$ . Indeed, the other two-rings within the tangle also form  $3_1^+$  knots. Since  $3_1^+$  is topologically chiral, this self-entangled polyhedron is also topologically chiral.

This example is one member of an infinite family of  $[\frac{\pm t}{3}]_{\theta}^3$  tangled  $\theta$ -polyhedra. Generic twists,  $t$ , induce self-entangled  $\theta$ -polyhedra with one component. Triple-helical windings  $[\frac{t}{3}]_{\theta}^3$  and  $[\frac{-t}{3}]_{\theta}^3$  are chiral enantiomers, for arbitrary  $t$ . However, if  $t$  is a multiple of three (i.e.,  $\text{mod}_3(t) = 0$ ), the polyhedral tangle is a four-component link rather than a knot, as shown in Fig. 3. Three of those components are topological loops (colored red, green, and blue in Fig. 3); the fourth component is a  $\theta$ -graph (colored black in Fig. 3).

Similarly, generic polyhedral tangles wound on the bitorus, whose skeleton is the  $\theta$ -graph,  $[\frac{t}{2k+1}]_{\theta}^3$  with coprime twist  $t$  and track number  $2k + 1$ , induce a chiral self-entangled  $\theta$ -polyhedron with symmetry  $233$ . If  $\text{mod}_{2k+1}(t) = 0$ , the tangle is a catenated link with  $2(k + 1)$  components, including a single  $\theta$  graph and  $2k + 1$  unbranched loops. A further set of isolated cases, whose track numbers,  $2k + 1$ , satisfy  $\text{mod}_t(2k + 1) = 0$ , also form links, rather than a single-component knotted  $\theta$  graph. For example, the  $[\frac{3}{9}]_{\theta}^3$  tangle is also a four-component link, like those in Fig. 3.

Generic tangles described by  $2k + 1$ -strand helical windings on a polytorus whose skeleton is an  $\{f, z\}$  polyhedron can be traced out on the page by first drawing a planar Schlegel diagram of the polyhedron,  $P$ , containing  $E$  edges. Edges of the Schlegel diagram describe the central track, of track-index zero. The remaining  $\pm k$  tracks on either side of the central track (with indices  $\pm(1 - k)$ ) are joined end-to-end, forming  $k$  concentric loops within each  $f$ -sided face of the original skeleton. The resulting diagram describes the untwisted tangle,  $[\frac{0}{2k+1}]_P^E$ . Twists  $t$  are generated by joining incoming to outgoing ports to effect a  $2k + 1$ -helix of twist  $t$ . For example, a seven-track diagram ( $k = 3$ ) on the octahedron ( $P = \text{oct}$ ) is illustrated in Fig. 4A. A single track on a tangled configuration with twist  $t = 2$ , forming the tangle  $[\frac{2}{7}]_{\text{oct}}^{12}$ , is traced out in Fig. 4B.

We note that this construction schema induces branched strands, whose branchings coincide with vertices of the resulting polyhedral graph. A more rigorous analysis of the construction

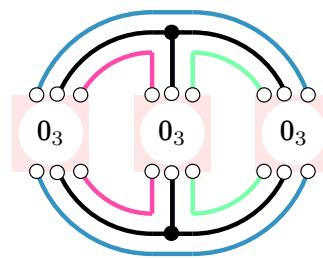


**Fig. 3.** Tangled polyhedra  $[\frac{\pm t_0}{3}]_{\theta}^3$ , where  $\text{mod}_3(t_0) = 0$ , with four distinct components colored red, blue, green, and black. These tangled polyhedra are four-component catenated entanglements of three unbranched loops (red, green, and blue) and a (branched)  $\theta$ -graph (black).

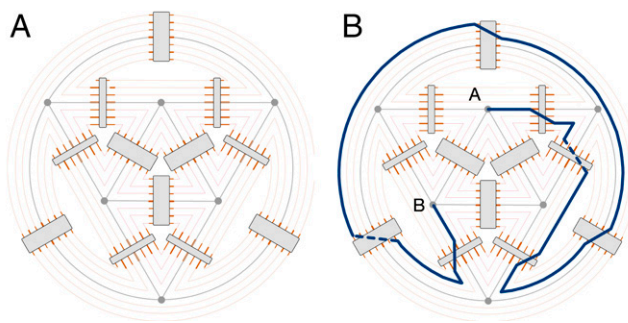


**Fig. 4.** (A) Construction of a seven-track polyhedral tangle on the octahedron,  $[\frac{t}{2k+1}]_{oct}^{12}$ , with arbitrary twist  $t$  and  $k = 3$ . A Schlegel diagram of the octahedral edge-net is drawn in gray, which passes through the central entrance and exit ports (index 0) of switch boxes interrupting each of the 12 edges. (B) An edge  $AB$  (shown in blue) of the  $[\frac{2}{7}]_{oct}^{12}$  tangle, connecting a pair of neighboring vertices on the octahedron via a helical winding traversing seven tubules of the octahedron. (Dashed line segments denote undercrossing paths.)

is possible by first building an unbranched winding of parallel twisted strands, forming twisted helices  $\frac{2t}{4k+2}$  wound around each tubule, and merging strand ends with those of neighboring tubules such that strands are combed to form parallel trajectories on the polytorus. Those unbranched railways are circuit double-covers (30) of the branched constructions we describe, with component helices  $\frac{t}{2k+1}$  wound around each tubule.

### Topologies of 2fz Tangled Polyhedra

Polyhedral tangles wound on tubified skeletons of the conventional Platonic polyhedra,  $P = \{f, z\}$ , also describe tangled polyhedra, whose topology and tangling depend on  $t$  and  $n = 2k + 1$ . All such tangled polyhedra,  $[\frac{t}{2k+1}]_P^E$ , can be embedded with symmetry 2fz. The most interesting examples are those whose fractions  $[\frac{t}{2k+1}]$  are “irreducible,” where  $t$  and  $2k + 1$  are coprime. From here on, we consider only those cases. Regardless of  $t$  and  $k$ ,  $[\frac{t}{2k+1}]_P^E$  irreducible tangles invariably consist of a single self-entangled  $\theta$ -graph only. However, irreducible tangles on tubified tetrahedra ( $P = tet$ ), cubes ( $P = cub$ ), octahedra ( $P = oct$ ), icosahedra ( $P = icos$ ), and dodecahedra ( $P = dodec$ ) form either single-component self-entangled polyhedra ( $P$ ) or multiple catenated congruent polyhedra (denoted  $P'$ , where  $P'$  is a graph minor of  $P$ ). The allowed topologies, characterized by the number of component graphs within the tangle ( $L$ ) and constituent polyhedra ( $P'$ ), are severely constrained. (Notice that if  $L = 1$ ,  $P' = P$ .)

Just as a helical edge of an irreducible three-track tangled  $\theta$ -polyhedron traverses three tubules from vertex to vertex, any edge of an irreducible polyhedral tangle  $[\frac{t}{2k+1}]_P^E$  traverses  $2k + 1$  tubules of its underlying polytorus between graph vertices. (For example, edges of the  $[\frac{2}{7}]_{oct}^{12}$  tangle in Fig. 4B traverse seven tubules.) The helical winding of an edge around a \*2fz polytorus necessarily passes through an axis of twofold rotational symmetry of the underlying polytorus, located midway along its length, which exchanges the vertices at either end of the edge. (Otherwise, a pair of edges would span those vertices, giving a multi-graph, which does not correspond to a platonic polyhedron.) Pairs of vertices bounding edges of these 2fz polyhedral tangles are therefore necessarily related by isometries about axes of rotational symmetry of even order. Further, since the edges traverse  $2k + 1$  tubules, they can be projected onto their underlying polyhedral skeleton  $P$  to form walks passing through  $2k + 1$  edges of  $P$ . Since  $2k + 1$  is odd, those axes must pass through midpoints of edges of  $P$ . (That constraint rules out generic

even-order rotation axes passing through vertices of  $P$ .) Consider, for example, tangled cubes,  $[\frac{t}{2k+1}]_{cub}^{12}$ , with symmetry 234. In that case, admissible rotation axes are parallel to the face-diagonals of the cube, passing through its center. Examples of allowed edges of these tangles, projected onto the edges of the underlying cube skeleton, traversing three and five tubules of the tubified cube (i.e.,  $k = 1, 2$ ), are illustrated in Fig. 5 A and B, respectively. Indeed, regardless of the starting vertex and choice of rotation axis, vertex pairs ( $A$  and  $B$ ) at either end of edges in  $[\frac{t}{2k+1}]_{cub}^{12}$  tangles with symmetry 234 can only be located 1) at both ends of an edge of the untangled cube (as in Fig. 5B) or 2) at both ends of a body diagonal (Fig. 5A). In the former case, the orbit of tangled edges by 234 isometries results in just one component net in the tangle: a self-entangled cube. On the other hand, if they lie on a body diagonal, the orbit generates four catenated  $\theta$ -polyhedra. (A third candidate topology for tangled cubes, a pair of catenated tetrahedra, is excluded, since edges joining adjacent tetrahedral vertices traverse an even number of tubules.) In summary,  $[\frac{t}{2k+1}]_{cub}^{12}$  tangled cubes allow the following topologies only: self-entangled cubes ( $L = 1$ ,  $P' = P = cub$ ) or catenations of four  $\theta_3$ -polyhedra ( $L = 4$ ,  $P' = \theta_3$ ).

Similar considerations dictate allowed topologies of other self-entangled or mutually tangled polyhedra,  $[\frac{t}{2k+1}]_P^E$ , with symmetries 2fz and irreducible  $\frac{t}{2k+1}$ . Tangles on the dodecahedral polytorus exhibit the broadest variety of topologies, forming catenated  $\theta_3$ -polyhedra ( $L = 10$ ) and catenated tetrahedra ( $L = 5$ ), as well as a self-entangled dodecahedron ( $L = 1$ ). Self-entangled octahedra, cubes, and icosahedra ( $L = 1$ ) exist for certain values of  $t, k$  only; otherwise, catenated  $\theta_z$ -polyhedra are formed on the octahedral polytorus ( $L = 3$ ,  $P = oct$ ,  $P' = \theta_4$ ), the cube polytorus ( $L = 4$ ,  $P = cub$ ,  $P' = \theta_3$ ), and the icosahedral polytorus ( $L = 6$ ,  $P = icos$ ,  $P' = \theta_5$ ). In contrast, all irreducible tangled tetrahedra,  $[\frac{t}{2k+1}]_{tet}^6$  share common topology, regardless of  $t$  and  $k$ : a self-entangled tetrahedron ( $L = 1$ ).

Though the topologies of these entangled 2fz polyhedra are limited, the number of distinct isotopes is unbounded. (Recall that equivalent isotopes or tangles can be morphed into each other by ambient isotopies; distinct cases cannot.) Here, we deduce the simpler isotopes only, limited by the following considerations. First, we ignore  $k = t = 0$ , since those untwisted 2fz polyhedra can be further symmetrized to form the untangled Platonic polyhedra, with symmetry \*2fz. Second, we consider only irreducible cases, where  $t$  and  $2k + 1$  are coprime, for reasons described above. Third, tangling of a polyhedron  $[\frac{t}{2k+1}]_P^E$  is that of its chiral enantiomer  $[\frac{-t}{2k+1}]_P^E$  modulo a reflection. Lastly, tangled polyhedra  $[\frac{\pm(t \pm j(2k+1))}{2k+1}]_P^E$  (where  $j$  is an integer) share common edge topology—though likely not tangling—regardless

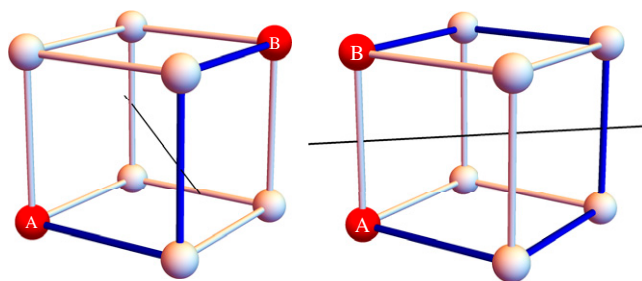


**Fig. 5.** Two examples of edges  $AB$  in tangled cubes,  $[\frac{t}{2k+1}]_{cub}^{12}$  (drawn in blue) projected onto edges of the underlying cube polytorus skeleton, with  $k = 1$  (A) and  $k = 2$  (B). Twofold axes of rotational symmetry of the underlying Platonic cube skeleton, drawn as black lines, pass through the midpoints of  $AB$ .

of  $j$ , since incrementing  $j$  adds  $2\pi$  “Dehn twists” (31) within the switch, but preserves the entrance and exit ports at each switch. Thus, for example, seven-track tangled polyhedra  $[\frac{t}{7}]_P^E$  fall into three groups of chiral pairs:  $[\frac{\pm 1 \pm 7j}{7}]_P^E$  and  $[\frac{\pm 6 \pm 7j}{7}]_P^E$ ;  $[\frac{\pm 2 \pm 7j}{7}]_P^E$  and  $[\frac{\pm 5 \pm 7j}{7}]_P^E$ ; and  $[\frac{\pm 3 \pm 7j}{7}]_P^E$  and  $[\frac{\pm 4 \pm 7j}{7}]_P^E$ . We consider just one enantiomer in each class, so all seven-track topologies are found from the following cases:  $[\frac{1}{7}]_P^E$ ,  $[\frac{2}{7}]_P^E$ , and  $[\frac{3}{7}]_P^E$ . It turns out that the full spectrum of possible topologies of these 2fz tangled polyhedra is generated by three-, five-, and seven-track polyhedra, so we have analyzed tangles with  $k < 4$  only.

### Self-Entangled 2fz Polyhedra

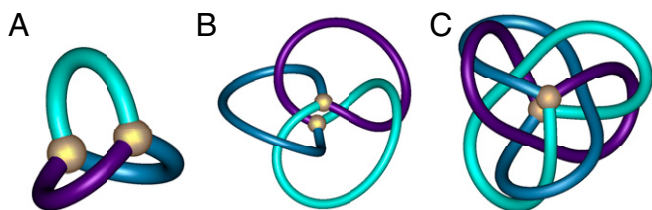
Consider first tangled polyhedra that result from winding an odd number of tracks ( $2k + 1$ ) around the three edges of a tubified  $\theta_3$  polyhedron,  $[\frac{t}{2k+1}]_\theta^3$ . Those windings are chiral and can be embedded with maximal symmetry 223. As noted above, these form a single-component tangled  $\theta$ -polyhedron, regardless of (coprime)  $t$  and  $n$ . The simplest (nontrivial) tangles,  $[\frac{1}{3}]_\theta^3$  and  $[\frac{2}{3}]_\theta^3$ , are shown in Fig. 6 B and C, along with the trivial tangle,  $[\frac{0}{3}]_\theta^3$  (Fig. 6A).

It is clear that the  $[\frac{2}{3}]_\theta^3$  case is a distinct isotope to the trivial (untangled)  $\theta$ -polyhedron since, in contrast to the untangled  $\theta$ -polyhedron, all two-rings are knotted, forming like-handed trefoils, as shown in Fig. 7 A–C. Its enantiomer,  $[\frac{-2}{3}]_\theta^3$ , generates trefoils of the opposite hand. (For brevity, we describe the two-ring knots of the enantiomers, labeled  $[\frac{\pm 2}{3}]_\theta^3$  by the label  $3_\theta^{\pm 2}$ .) In contrast, all cycles in the  $[\frac{\pm 1}{3}]_\theta^3$  tangles are unknotted (Fig. 7 D–F). Nevertheless, they form an enantiomeric pair of distinct isotopes to the trivial (untangled) embedding,  $[\frac{0}{3}]_\theta^3$ , since they cannot be untangled to form the trivial embedding without cutting and regluing edges. These  $[\frac{\pm 1}{3}]_\theta^3$  tangles are the simplest examples of an infinite class of chiral tangles explored previously, classified as universal three-ravels (6). Interestingly, one enantiomer has been realized at the atomic (Å) scale in an organometallic molecule, with stoichiometry  $C_{312}H_{336}Fe_8O_{60}$  and symmetry 223 (Schoenflies symbol  $D_3$ ) (7).

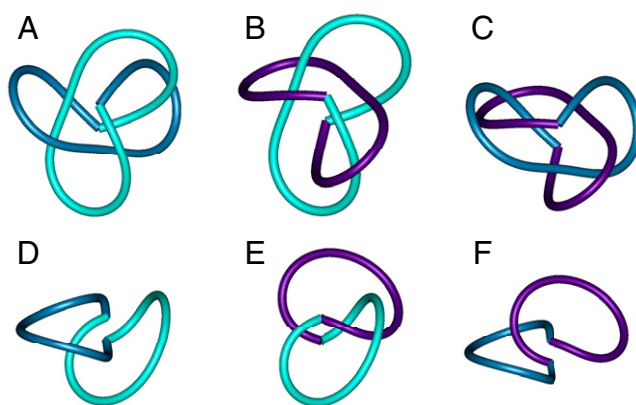
Self-entangled platonic polyhedra with topologies  $L = 1, P = P'$ , including  $\{f, z\} = \{3, 3\}$  ( $P = tet$ ),  $\{3, 4\}$  ( $P = oct$ ),  $\{4, 3\}$  ( $P = cub$ ),  $\{3, 5\}$  ( $P = icos$ ), and  $\{5, 3\}$  ( $P = dodec$ ), are generated by winding  $2k + 1$ -track helices on each tubule of the polytorus formed by inflating that same Platonic polyhedron  $P$ . The simplest resulting self-entangled maximally symmetric platonic polyhedra, with lowest indices  $t, k$ , are shown in Fig. 8.

Table 1 lists all of the self-entangled platonic polyhedra,  $[\frac{t}{2k+1}]_P^E$ , where  $k \leq 3$ , and  $t$  is limited to the values discussed in *Topologies of 2fz Tangled Polyhedra*.

It is possible that all tangles of a given platonic polyhedron  $P$  with distinct labels  $t$  and  $k$  build distinct isotopes. Nearly all the



**Fig. 6.** (A) Relaxed, symmetrized (\*223) embedding of the untangled  $\theta$ -polyhedron  $[\frac{0}{3}]_\theta^3$ . (B) The chiral (223) raveled tangle of the  $\theta$ -polyhedron,  $[\frac{1}{3}]_\theta^3$ . (C) The simplest chiral (223) knotted tangle,  $[\frac{2}{3}]_\theta^3$  (cf. Fig. 2).



**Fig. 7.** (A–C) Knotted ( $3_1^+$ ) trefoils in the  $[\frac{2}{3}]_\theta^3$  tangles. (D–F) Unknotted embeddings of loops in the  $[\frac{1}{3}]_\theta^3$  tangles.

( $f$ -)rings of edges in these tangled polyhedra form distinct knots, depending on  $t$  and  $k$ , as listed in Table 1. However, some isotopes cannot be distinguished on that basis, namely, the  $\theta$

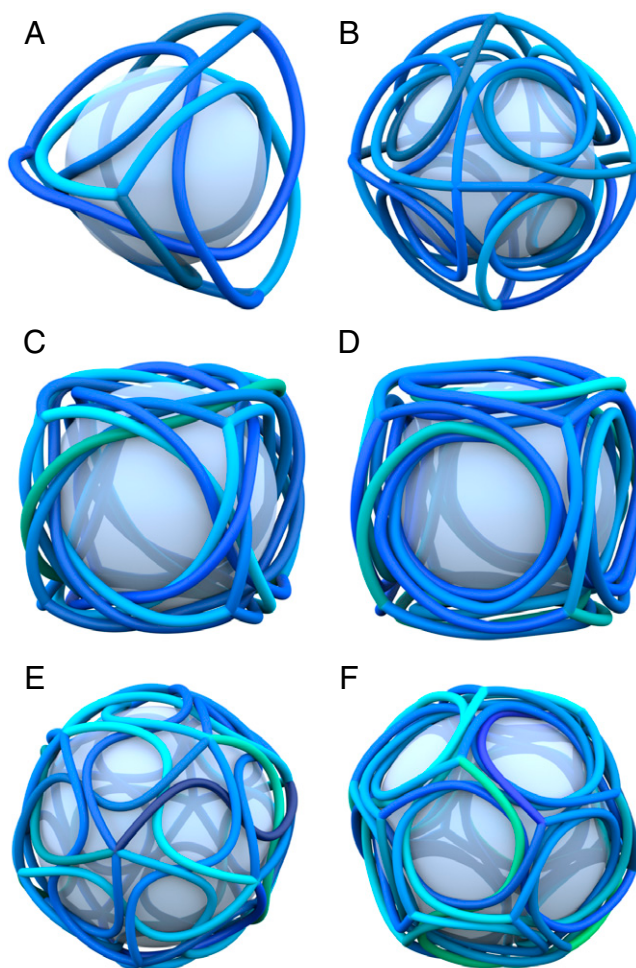


**Fig. 8.** The simplest tangled vertex-, edge-, and face-transitive platonic polyhedra built from three-, five-, and seven-strand helices. (A) The chiral tangled tetrahedron,  $[\frac{1}{3}]_{tet}^6$ , with symmetry 233. (B) The chiral tangled octahedron,  $[\frac{1}{5}]_{oct}^{12}$ , with symmetry 234. (C and D) A pair of vertex-, edge-, and face-transitive tangled cubes,  $[\frac{2}{5}]_{cub}^{12}$  and  $[\frac{1}{7}]_{cub}^{12}$ , with symmetry 234. (E and F) A tangled icosahedron,  $[\frac{1}{3}]_{icos}^{30}$ , and tangled dodecahedron,  $[\frac{1}{5}]_{dodec}^{30}$ ; both embeddings have chiral symmetry 235. Note that vertices of these polyhedra coincide with those of their untangled Platonic analogs.

**Table 1. Single-component self-entangled platonic  $\{f, z\}$  polyhedra  $[\frac{t}{2k+1}]_P^E$  formed by windings on tubified dodecahedra, icosahedra, cubes, octahedra, and tetrahedra**

Polyhedron $P$	Symmetry	$[\frac{t}{2k+1}]_P^E$	Topology	$N_\times$	$f$ -ring knot
Dodecahedron	235 ( $I$ )	$[\frac{\pm 1}{5}]_P^{30}, [\frac{\pm 4}{5}]_P^{30}, \dots$		120, 480, ...	$5_1^\pm, \dots$
		$[\frac{\pm 2}{7}]_P^{30}, [\frac{\pm 5}{7}]_P^{30}, \dots$		360, 900, ...	$10_{123}^\pm, \dots$
Icosahedron	235 ( $I$ )	$[\frac{\pm 1}{3}]_P^{30}, [\frac{\pm 2}{3}]_P^{30}, \dots$		60, 120, ...	$0_1, \dots$
		$[\frac{\pm 1}{5}]_P^{30}, [\frac{\pm 4}{5}]_P^{30}, \dots$		120, 480, ...	$3_1^\pm, \dots$
		$[\frac{\pm 1}{7}]_P^{30}, [\frac{\pm 6}{7}]_P^{30}, \dots$		180, 1,080, ...	$8_{19}^\pm, \dots$
		$[\frac{\pm 3}{7}]_P^{30}, [\frac{\pm 4}{7}]_P^{30}, \dots$		540, 720, ...	$10_{123}^\pm, \dots$
Cube	234 ( $O$ )	$[\frac{\pm 2}{5}]_P^{12}, [\frac{\pm 3}{5}]_P^{30}, \dots$		96, 144, ...	$8_{18}^\pm, \dots$
		$[\frac{\pm t}{7}]_P^{12}$		72t	$8_{19}^\pm (t=1), \dots$
Octahedron	234 ( $O$ )	$[\frac{\pm t}{5}]_P^{12}$		48t	$3_1^\pm, 3_1^\mp (t=1, 2), \dots$
		$[\frac{\pm t}{7}]_P^{12}$		72t	$8_{19}^\pm, 9_{49}^\pm (t=1, 2), \dots$
Tetrahedron	233 ( $T$ )	$[\frac{\pm 1}{3}]_P^6, [\frac{\pm 2}{3}]_P^6, \dots$		12, 24, ...	$3_1^\pm, \dots$
		$[\frac{\pm t}{5}]_P^6$		24t	$3_1^\mp, 9_{47}^\pm (t=1, 2), \dots$
		$[\frac{\pm t}{7}]_P^6$		72t	$8_{19}^\pm (t=1), \dots$
$\theta$	223 ( $D_3$ )	$[\frac{\pm 1}{3}]_P^3, [\frac{\pm 2}{3}]_P^3, \dots$		6, 12, ...	$0_1, 3_1^\pm, \dots$
		$[\frac{\pm 1}{5}]_P^3, [\frac{\pm 4}{5}]_P^3, \dots$		12, 48, ...	$3_1^\pm, \dots$
		$[\frac{\pm 2}{5}]_P^3, [\frac{\pm 3}{5}]_P^3, \dots$		24, 36, ...	$6_1^\pm, \dots$
		$[\frac{\pm t}{7}]_P^3$		18t	$3_1^\pm, 8_{19}^\pm (t=1, 2), \dots$

Crossing numbers ( $N_\times$ ) are listed for planar projections of the tangles drawn on Schlegel diagrams; these are not necessarily minimal. Their symmetries are listed as orbifold symbols  $2fz$  (and point groups  $I, O, T$ , or  $D_3$ ). Knots formed by face cycles are specified for lower twist cases (identified in parentheses). Higher-order tangled polyhedra, with twists  $t'$ , also form self-entangled polyhedra provided  $\text{mod}_{2k+1} t' = t$ . Note that our convention for + and - labeling of knots is arbitrary and listed only to distinguish like from unlike enantiomers of knots.

isotopes  $[\frac{\pm 2}{3}]_\theta^3, [\frac{\pm 1}{5}]_\theta^3$ , and  $[\frac{\pm 1}{7}]_\theta^3$ , tetrahedral isotopes  $[\frac{\pm 1}{3}]_\theta^6$  and  $[\frac{\pm 1}{5}]_\theta^6$ , and the octahedral isotopes  $[\frac{\pm 1}{5}]_\theta^{12}$  and  $[\frac{\pm 2}{5}]_\theta^{12}$ . The pair of tangled tetrahedra are necessarily distinct isotopes, as follows. On the one hand, the three-rings (topologically equivalent to those bounding faces of the untangled tetrahedron) in the  $[\frac{\pm 1}{3}]_\theta^6$  and  $[\frac{\pm 1}{5}]_\theta^6$  tangles form enantiomeric trefoils,  $3_1^\pm$  (i.e.,  $\pm \rightarrow \pm$ ) and  $3_1^\mp$  ( $\pm \rightarrow \mp$ ), respectively, so the ring knotting fails to definitively distinguish those isotopes. However, their four-sided skew Petrie polygons (32) form distinct knots: the prime trefoil knot ( $3_1^\pm$ ) and the composite pair of trefoils ( $3_1^\mp \# 3_1^\mp$ ) for the  $[\frac{\pm 1}{3}]_\theta^6$  and  $[\frac{\pm 1}{5}]_\theta^6$  tangles, respectively. Consequently, they are distinct (nontrivial) isotopes of the tetrahedron. Similarly, three-rings in the tangled octahedra  $[\frac{\pm 1}{5}]_\theta^{12}$  and  $[\frac{\pm 2}{5}]_\theta^{12}$  form identical  $3_1^\pm$  trefoils, whereas their six-sided skew Petrie polygons describe distinct knots, namely, ( $3_1^\mp \# 3_1^\mp \# 3_1^\mp$ ) and a nonalternating 12-crossing knot.

Since two-rings in the tangled  $\theta$ -polyhedra  $[\frac{\pm 1}{5}]_\theta^3$  and  $[\frac{\pm 1}{7}]_\theta^3$  are trefoils, those cases are distinct isotopes to the trivial isotope,  $[0]_\theta^3$ , as well as the raveled  $[\frac{\pm 1}{3}]_\theta^3$  isotope, though indistinguishable from the  $[\frac{\pm 2}{3}]_\theta^3$  knotted isotope. Since  $[\frac{\pm 2}{3}]_\theta^3, [\frac{1}{5}]_\theta^3$  and  $[\frac{1}{7}]_\theta^3$  contain trefoils only, they cannot be distinguished on the basis of their knotted cycles. We therefore explored so-called “tight” embeddings of these tangled polyhedra. Tight knots minimize the total edge length of the knots realized as unit diameter tubes that do not overlap (33, 34). A numerical procedure to estimate tight embeddings of graphs generalize that concept, admitting branched vertices (35). This approach is useful, assuming distinct

isotopes form noncongruent tight embeddings. That assumption holds for most knots although there are some exceptions (34), as well as simpler graph embeddings (35). Numerical realizations of tight embeddings of the  $[\frac{2}{3}]_\theta^3, [\frac{1}{5}]_\theta^3$ , and  $[\frac{1}{7}]_\theta^3$  tangles are shown in Fig. 9. Since those embeddings differ significantly, with distinct total lengths, it is very likely that all three tangled embeddings of the  $\theta$ -graph are distinct isotopes.

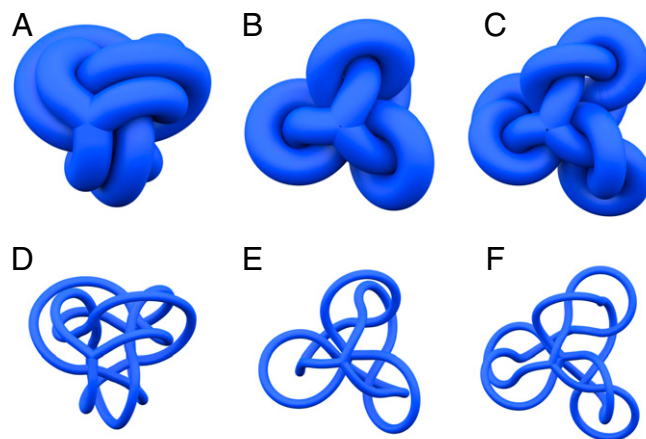


**Fig. 9.** (A–C) Tight embeddings of  $[\frac{2}{3}]_\theta^3$  (A),  $[\frac{1}{5}]_\theta^3$  (B), and  $[\frac{1}{7}]_\theta^3$  (C) tangled  $\theta$ -polyhedra, with lengths 47.10, 36.25, and 48.20, respectively. (D–F) The same embeddings traced with reduced edge diameter, revealing their very different tight geometries.

In summary, for all the cases explored to date, retuning the component helices wound on a polyhedron  $P$  by adjusting  $t$  and/or  $k$  induces a different  $2fz$  isotope,  $\left[\frac{t}{2k+1}\right]_P^E$ .

All of these self-entangled embeddings are geometrically chiral, leading to the question of their topological chirality; i.e., can they be deformed into their enantiomer by some deformation that does not include phantom crossings (36)? Topological chirality of these  $2fz$  tangles is assured, provided they contain (topologically chiral) knotted  $f$ -rings and just one knot enantiomer is present in the graph embedding. Nearly all the polyhedral tangles whose  $f$ -ring knots are listed in Table 1 fulfill these criteria. There are just two exceptions among the lower-index tangles in Table 1: the raveled  $\theta$ -polyhedron  $\left[\frac{1}{3}\right]_{\theta}^3$  and the tangled icosahedron  $\left[\frac{1}{3}\right]_{icos}^{30}$ . Nevertheless, both exceptions are also topologically chiral. The  $\left[\frac{1}{3}\right]_{\theta}^3$  tangle is among Moriuchi's census of  $\theta$ -graphs (5<sub>1</sub>), all of which are topologically chiral (37). Although isolated three-rings of the icosahedral isotope are unknotted, triplets of those rings form  $6_3^3$  links, which are topologically chiral (38). All of these lower-index, self-entangled platonic polyhedra are therefore topologically chiral. We conjecture that all single-component self-entangled platonic polyhedra  $\left[\frac{t}{2k+1}\right]_P^E$  (with coprime  $t$  and  $k$ ) are topologically chiral.

### The $2fz$ Isotopes of Self-Entangled Polyhedra Are Maximally Symmetric

These odd-order helical windings realize very symmetric tangled polyhedra ( $2fz$ , with two flags). Nevertheless, they are slightly less symmetric than those of the (untangled) Platonic polyhedra, realized with just one flag, forming patterns with symmetry  $*2fz$ . In order to rule out flag-transitive tangled polyhedra, it is necessary to establish that any embedding of an  $\{f, z\}$  polyhedral graph with symmetry  $*2fz$  is necessarily untangled. That is readily demonstrated for the simplest polyhedral topology, namely, the  $\theta$ -polyhedron, for which  $\{f, z\} = \{2, 3\}$ , as follows. Assume that a  $\theta$ -polyhedron is realized with symmetry  $*223$ , in which case its pair of antipodal three-valent vertices (marked  $A$  and  $B$  in Fig. 10A) lie on a common threefold axis of rotational symmetry, displaced equally from the center, which lies on three axes of twofold rotational symmetry. The polyhedron contains three mirror planes,  $\Pi_1, \Pi_2,$  and  $\Pi_3$ , each split into half-planes,  $\Pi_i^+$  and  $\Pi_i^-$ , intersecting along the common axis  $AB$ , as shown in Fig. 10A. All three curved edges of the  $\theta$ -polyhedron are necessarily confined to mirror planes; e.g.,  $Aabb$  lies in  $\Pi_1$ . (Clearly, their tangent vectors at  $A$  and  $B$  lie in  $\Pi_1$ , since otherwise,  $A$  and  $B$  would be six-valent. If the edge leaves  $\Pi_1$  somewhere along its length, a forbidden three-valent vertex is generated by that mirror; therefore, the entire edge  $Aabb$  lies in  $\Pi_1$ .) If the edge  $Aabb$  intersects the threefold line  $AB$ , forbidden three-valent vertices are formed at intersections  $a$  and  $b$ , so  $Aabb$  is confined to the half-plane  $\Pi_1^+$ , as in Fig. 10B. Similarly, the other pair of edges are located in half-planes  $\Pi_2^+$  and  $\Pi_3^+$ , such that all three half-planes subtend angles of  $\frac{2\pi}{3}$  with each other. All edges can therefore be morphed within their respective half-planes to lie along meridians of a sphere without intersections (Fig. 10C). It follows that any embedding of the  $\theta$ -polyhedron with symmetry  $*223$  is necessarily untangled.

Similar reasoning proves that embeddings of  $\{f, z\}$  graphs with symmetry  $*2fz$ , where  $\{f, z\} = \{3, 3\}, \{3, 4\}, \{4, 3\}, \{3, 5\}$ , or  $\{5, 3\}$ , are also necessarily untangled, forming equivalent isotopes to the standard Platonic tetrahedron, octahedron, cube, icosahedron, or dodecahedron, respectively. It follows that all tangled isotopes of polyhedral graphs  $\{f, z\}$  have at least two flags and the  $2fz$  constructions of  $\left[\frac{t}{2k+1}\right]_P^E$  tangles outlined above are maximally symmetric.

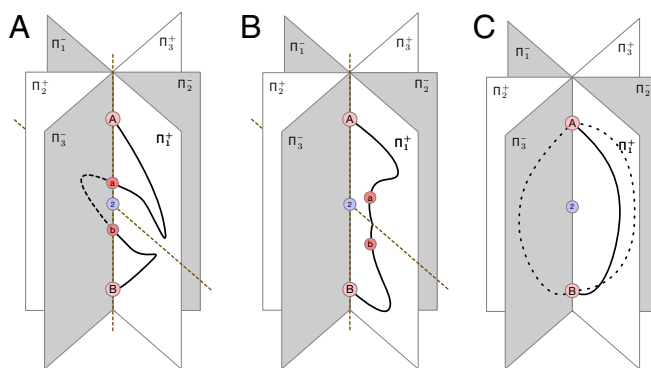


**Fig. 10.** Three mirror planes of a  $\theta$ -polyhedron with symmetry  $*223$  labeled  $\Pi_1, \Pi_2,$  and  $\Pi_3$ , each split into half-planes  $\Pi_i^+$  and  $\Pi_i^-$ . They intersect along a common vertical axis of threefold rotational symmetry passing through (red) points marked  $A, a, b, B$ .  $A$  and  $B$  are located at equal (unit) distance from the (blue) site marked  $2$ , located on the threefold axis  $AB$  and a horizontal mirror plane, containing three orthogonal axes of twofold rotational symmetry. (One of those axes is the dotted line, passing through  $2$ .) (A) A hypothetical edge of the  $\theta$ -polyhedron,  $Aabb$ , whose tangent vector at  $A$  and  $B$  must lie in plane  $\Pi_1$ , since  $A, B$  are three-valent vertices. If  $a, b$  also lie on the axis  $AB$ , they induce forbidden three-valent vertices. (B) A valid edge  $Aabb$  of the  $*223$   $\theta$ -polyhedron therefore lies entirely within the (white) half-plane  $\Pi_1^+$ . (C) Since all three edges are confined to their (white) half-planes, the  $Aabb$  edge can be deformed to lie along a meridian of a unit sphere centered at  $2$ , with poles  $A$  and  $B$ . By symmetry, all three edges can be similarly deformed, so the  $\theta$ -polyhedral edges can be deformed to lie on three half-planes without edge-crossings. It follows that any embedding of the  $\theta$ -graph  $\{2, 3\}$  with symmetry  $*223$  is untangled.

### Catenated (Compound) $2fz$ Platonic Polyhedra

Self-entangled polyhedra share identical graph topologies (though not entanglements) with their Platonic precursors: Their entangled graphs can be morphed into a single copy of one of the familiar Platonic polyhedral embeddings via some deformation, which includes edges passing through each other (phantom crossings). Those single-component polyhedral graphs are realized for  $\left[\frac{t}{2k+1}\right]_P^E$  tangles, provided  $t$  and  $k$  are equal to those listed in Table 1. Otherwise, the polyhedral tangles  $\left[\frac{t}{2k+1}\right]_P^E$  lead to entanglements containing multiple, equivalent graphs,  $P' \neq P$ , rather than a single self-entangled polyhedron. The resulting “polyhedral links” are listed in Table 2.

Among the low-index tangles analyzed here, the most spectacular linked polyhedra are those resulting from three- and seven-track windings on the dodecahedral polytorus, which induce five disjoint, but mutually catenated, tetrahedra. The simplest isotope,  $\left[\frac{1}{3}\right]_{dodec}^{30}$ , is identical to the well-known regular compound tetrahedron, labeled  $\{5, 3\}[5\{3, 3\}]\{3, 5\}$  by Coxeter (39). The embedding induced by the  $\left[\frac{1}{3}\right]_{dodec}^{30}$  winding and the compound tetrahedron are shown in Fig. 11. Both embeddings are chiral, with symmetry 235. The helical edges of the  $\left[\frac{1}{3}\right]_{dodec}^{30}$  embedding inherited from the triple-helical winding impose 233 symmetry on each component tetrahedron in the tangle, whereas the straight edge in the compound polyhedron result in enhanced symmetry ( $*233$ ) for each tetrahedron. Among all  $2fz$  tangles  $\left[\frac{t}{2k+1}\right]_P^E$ , this is the sole isotope we have identified whose edges can be rectified without phantom crossings.

The remaining  $\left[\frac{t}{2k+1}\right]_P^E$  polyhedral links, wound around tubified dodecahedra, icosahedra, cubes, and octahedra, are catenations of three-, four-, and five-valent  $\theta_z$  polyhedra (i.e.,  $P' = \theta_z$ , where  $z = 3, 4, 5$ ), listed in Table 2. Some of the simpler cases are shown in Fig. 12. Like the self-entangled examples previously described, the vertices in each mutually catenated  $2fz$

**Table 2. Vertex and edge-transitive catenations of multiple equivalent polyhedra  $P'$  formed from  $2fz$  polyhedral tangles on tubified polyhedra  $P$ ,  $\left[\frac{t}{2k+1}\right]_P^E$**

Polytorus skeleton $P$	Symmetries	$\left[\frac{t}{2k+1}\right]_P^E$	Topology	$P'$	#
Dodecahedron	235–234 ( $I - T$ )	$\left[\frac{\pm 1}{3}\right]_P^{30\ddagger}, \left[\frac{\pm 2}{3}\right]_P^{30}, \dots$		{3, 3}	5
	235–223 ( $I - D_3$ )	$\left[\frac{\pm 2}{5}\right]_P^{30}, \left[\frac{\pm 3}{5}\right]_P^{30}, \dots$		{2, 3}	10
	235–234 ( $I - T$ )	$\left[\frac{\pm 1}{7}\right]_P^{30}, \left[\frac{\pm 6}{7}\right]_P^{30}, \dots$		{3, 3}	5
	235–234 ( $I - T$ )	$\left[\frac{\pm 3}{7}\right]_P^{30}, \left[\frac{\pm 4}{7}\right]_P^{30}, \dots$		{3, 3}	5
Icosahedron	235–225 ( $I - D_5$ )	$\left[\frac{\pm 2}{5}\right]_P^{30}, \left[\frac{\pm 3}{5}\right]_P^{30}, \dots$		{2, 5}	6
Cube	234–223 ( $O - D_3$ )	$\left[\frac{\pm 1}{3}\right]_P^{12}, \left[\frac{\pm 2}{3}\right]_P^{12}, \dots$		{2, 3}	4
	234–223 ( $O - D_3$ )	$\left[\frac{\pm 1}{5}\right]_P^{12}, \left[\frac{\pm 4}{5}\right]_P^{12}, \dots$		{2, 3}	4
Octahedron	234–224 ( $O - D_4$ )	$\left[\frac{\pm 1}{3}\right]_P^{12}, \left[\frac{\pm 2}{3}\right]_P^{12}, \dots$		{2, 4}	3

Each component  $P'$  has topology  $f, z$ , listed in column 4. The number of discrete polyhedra  $P'$  is listed as # in column 5. All structures can be embedded with uncolored-colored symmetries  $2f''z-22z$ . (The tangle marked  $\ddagger$  lifts to a more symmetric embedding.)

polyhedral complex coincide with vertices of the  $*2fz$  Platonic polyhedral skeleton of the underlying polytorus,  $P$ . The  $\theta_z$  links partition vertices into antipodal pairs; each pair belongs to a single  $\theta_z$  polyhedron. All  $\theta_z$  links are embedded such that each  $\theta_z$  component has symmetry  $22z$ . More generally, an uncolored  $L$ -component link  $\left[\frac{t}{2k+1}\right]_P^E$ , with symmetry  $2fz$  (where  $P$  has Schläfli symbol  $\{f, z\}$ ), leads to a colored pattern, formed by coloring each component in the link differently. That colored pattern has reduced symmetries: either  $22z$  for  $\theta_z$  catenations or

234 for catenations of tetrahedra. (In either case, the uncolored symmetry is an index- $L$  supergroup of its colored symmetry.)

### Discussion

These polyhedral isotopes realize the most symmetric embeddings in three-space for all tangled polyhedral nets whose edge-graphs correspond to those of conventional Platonic polyhedra (and  $\theta_z$ -polyhedra). Their constituent helices contain an odd number of strands, and related patterns can be constructed by winding even-stranded helices around the same polytori, with Platonic skeletons. For example,  $\left[\frac{\pm 1}{10}\right]_{tet}^6$  and  $\left[\frac{\pm 3}{6}\right]_{tet}^6$  induce self-catenated cube isotopes. Neither isotope is equivalent to the isotopes shown in Fig. 8 C and D. Both the 6- and 10-helical examples have symmetry 233 ( $T$ ), lower than that of the odd-track self-entangled cubes, which display 234 ( $O$ ) symmetry. Note however, that the isotope generated by a tangle signature  $\left[\frac{t}{2k+1}\right]_P^E$  is not an invariant of the graph isotope.

For example, the isotope induced by the tangle  $\left[\frac{\frac{1}{2}(2k+1)}{2t}\right]_\theta^3$  is equivalent to  $\left[\frac{t}{2k+1}\right]_\theta^3$ . Tightening the five- and seven-strand  $\theta$ -polyhedral tangles  $\left[\frac{1}{5}\right]_\theta^3$  and  $\left[\frac{1}{7}\right]_\theta^3$  induce “flyped” embeddings, where the tangle is turned in on itself, analogous to turning a part of a sock inside-out.\* Those embeddings have signatures  $\left[\frac{5}{2}\right]_\theta^3$  and  $\left[\frac{7}{2}\right]_\theta^3$ , respectively—characteristic of double-helices. Indeed, two-stranded (double-)helices wound around the edges of the  $\theta$ -skeleton are visible in Fig. 9 B and E and C and F.

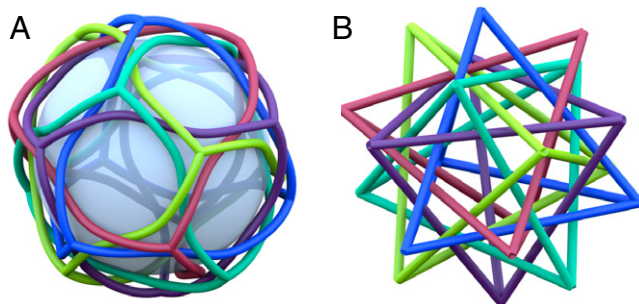


**Fig. 11.** (A) The dodecahedral winding of triple-helices,  $\left[\frac{1}{3}\right]_{dodec}^{30}$ , with chiral symmetry 235, made of five catenated tetrahedra, each with symmetry 233. (B) The edges in A can be rectified without passing edges through each other, forming a regular compound polyhedron, labeled  $\{5, 3\}5\{3, 3\}\{3, 5\}$  by Coxeter, with uncolored-colored symmetries 235–\*233.

\*Not dissimilar to the flype maneuver introduced by Tait to explore knots (13).

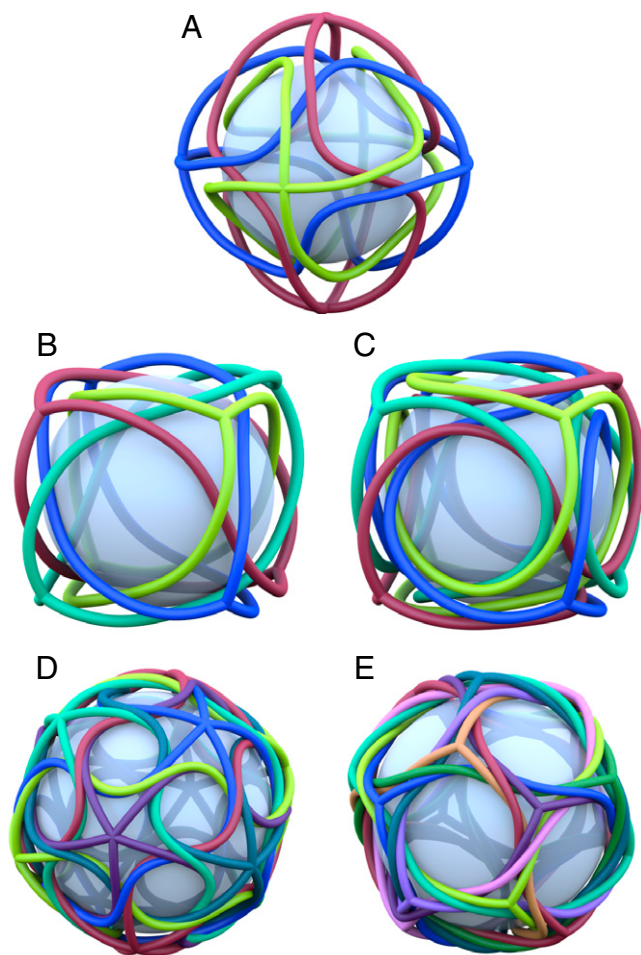


**Fig. 12.** Compound 2fz polyhedra, containing catenated copies of  $\theta_z$  polyhedra. (A) The octahedral tangle,  $[\frac{1}{3}]_{oct}^{12}$ : a three-component catenation of  $\theta_4$  polyhedra, with uncolored-colored symmetries 234–224. (B and C) Cube tangles,  $[\frac{1}{3}]_{cub}^{12}$  and  $[\frac{1}{5}]_{cub}^{12}$ , containing four catenated  $\theta_3$ -polyhedra (symmetries 234–223). (D) The icosahedral tangle,  $[\frac{2}{5}]_{icos}^{30}$ , built of six catenated  $\theta_5$  polyhedra (symmetries 235–225). (E) The dodecahedral tangle,  $[\frac{2}{5}]_{dodec}^{30}$  including 10 catenated  $\theta$ -polyhedra (symmetries 235–223).

(Since strands traverse two edges of the  $\theta$ -skeleton between vertices, they twist by  $5\pi$  and  $7\pi$ , respectively, between vertices, passing from the top of the upper threefold junction in the tubified  $\theta$ , via the lower junction, to the underside of the same junction. The winding geometry of these tight configurations is best viewed in the three-dimensional .ply files found in *SI Appendix*.) Evidently, flying allows two alternative embeddings of the same isotope, with different tangle “signature”  $[\frac{t}{n}]_P^E$ . However, the constructions via helices with an odd number of strands,

$n = 2k + 1$ , are maximally symmetric, whereas flyped embeddings of the same isotope are not. Thus, the flyped, tight embeddings of an entangled  $\theta$ -graph via railways  $[\frac{5}{2}]_{\theta}^3$  and  $[\frac{7}{2}]_{\theta}^3$  have symmetry 33 ( $C_{3\nu}$ ), an index-2 subgroup of the embeddings,  $[\frac{1}{5}]_{\theta}^3$  and  $[\frac{1}{7}]_{\theta}^3$ , which exhibit symmetry 233.

These tangled polyhedra are attractive targets for materials science since their smoothly curved edges can be replaced by jointed stick-like edges with the same maximal symmetry, 2fz. (The number of jointed linear segments in each edge depends on the twist  $t$ .) Entangled and woven structures are of increasing relevance to synthetic chemical materials, from finite metal-organic molecules to extended COFs and MOFs, referred to at the opening of this paper. These materials are synthesized by assembly of identical chemical modules, leading to symmetric structures, with minimal transitivity (40, 41) (i.e., minimal number of symmetrically distinct edges and vertices). The 2fz polyhedral tangles introduced here are vertex- and edge-transitive, with just two flags. Therefore, they can be assembled from identical structural units containing a half-edge and a  $\frac{1}{z}$ -fraction of a single ( $z$ -branched) vertex. That feature is likely to be responsible for the formation of a molecule whose skeleton is equivalent to that of the simplest of all polyhedral tangles introduced in this paper,  $([\frac{1}{3}]_{\theta}^3)$  (1). More recent syntheses of entangled metal-organic molecules (2–5) have closely related and marginally less symmetric structures, which can also be described as (branched or unbranched) railways wound on polyhedra. Entangled infinite framework structures also emerge from these finite polyhedral tangles, which describe the embeddings of their quotient graphs [formed by replacing the infinite structure by a finite unit cell with periodic boundaries (42)]. We suspect that these structures are not limited to synthetic materials, given the report of chiral self-assemblies that resemble these polyhedral entanglements in biology. Simpler polyhedra formed by chiral “triskelion” assemblies of clathrin networks, which coat soft bilayer vesicles allowing cargo transport in vivo, are strikingly similar to  $\{f, 3\}$  tangled polyhedra enumerated here (43). Like synthetic organometallic materials, those biomolecular assemblies may be driven toward structurally homogeneous patterns, favoring very symmetric entanglements. Lastly, we note that all of these 2fz tangled polyhedral constructions are formed by assembling tubules, each wound by equivalent helices with  $2k + 1$  strands, into a polytorus. Thus, they can be viewed as ( $z$ -)branched helicates. Helicate chemistry, which has produced some of most complex molecular knots synthesized to date (44), is therefore a promising field in which to search for these most symmetric branched and tangled structures.

**Data Availability.** Data files (in .ply format) allowing three-dimensional viewing of some of the tangled polyhedra discussed in this paper, plus a table listing components numbers, have been deposited in GitHub ([https://github.com/stimhyde/platonic\\_tangles](https://github.com/stimhyde/platonic_tangles)). All other study data are included in the article and/or *SI Appendix*.

**ACKNOWLEDGMENTS.** We thank Rob Scharein for assistance with his (freely available) *KnotPlot* software, which was critical for initial exploration of these patterns.

- F. Li, J. K. Clegg, L. F. Lindoy, R. B. Macquart, G. V. Meehan, Metallosupramolecular self-assembly of a universal 3-ravel. *Nat. Commun.* **2**, 205 (2011).
- T. Sawada *et al.*, Metal-peptide rings form highly entangled topologically inequivalent frameworks with the same ring- and crossing-numbers. *Nat. Commun.* **10**, 921 (2019).
- Y. Domoto, M. Abe, T. Kikuchi, M. Fujita, Self-assembly of coordination polyhedra with highly entangled faces induced by metal-acetylene interactions. *Angew. Chem. Int. Ed. Engl.* **59**, 3450–3454 (2020).
- T. Sawada, M. Fujita, Orderly entangled nanostructures of metal-peptide strands. *Bull. Chem. Soc. Jpn.* **94**, 2342–2350 (2021).
- Y. Domoto, M. Abe, M. Fujita, A highly entangled  $(M_3 L_2)_8$  truncated cube from the anion-controlled oligomerization of a  $\pi$ -coordinated  $M_3 L_2$  subunit. *J. Am. Chem. Soc.* **143**, 8578–8582 (2021).
- A. F. Wells *et al.*, *Three Dimensional Nets and Polyhedra* (Wiley, Hoboken, NJ, 1977).
- S. Andersson *et al.*, The intrinsic curvature of solids. *Z. Kristallogr. Cryst. Mater.* **168**, 1–18 (1984).
- S. R. Batten, R. Robson, Interpenetrating nets: Ordered, periodic entanglement. *Angew. Chem. Int. Ed. Engl.* **37**, 1460–1494 (1998).
- I. Ino *et al.*, 2-D interwoven and 3-D 5-fold interpenetrating silver(I) complexes of 1-(isocyanidomethyl)-1H-benzotriazole and 1,3-bis(dicyanomethylidene)indan. *Inorg. Chem.* **39**, 4273–4279 (2000).
- E. V. Alexandrov, V. A. Blatov, D. M. Proserpio, A topological method for the classification of entanglements in crystal networks. *Acta Crystallogr. A* **68**, 484–493 (2012).
- Y. B. Zhang *et al.*, Single-crystal structure of a covalent organic framework. *J. Am. Chem. Soc.* **135**, 16336–16339 (2013).
- Y. Liu *et al.*, Weaving of organic threads into a crystalline covalent organic framework. *Science* **351**, 365–369 (2016).
- C. C. Adams, *The Knot Book* (American Mathematical Society, Providence, RI, 1994).

14. P. McMullen, E. Schulte, *Abstract Regular Polytopes* (Encyclopedia of Mathematics and its Applications, Cambridge University Press, Cambridge, UK, 2002), vol. 92.
15. S. T. Hyde, G. E. Schröder-Turk, Tangled (up in) cubes. *Acta Crystallogr. A* **63**, 186–197 (2007).
16. M. E. Evans, V. Robins, S. T. Hyde, Periodic entanglement I: Networks from hyperbolic reticulations. *Acta Crystallogr. A* **69**, 241–261 (2013).
17. L. Carlucci, G. Ciani, D. M. Proserpio, T. G. Mitina, V. A. Blatov, Entangled two-dimensional coordination networks: A general survey. *Chem. Rev.* **114**, 7557–7580 (2014).
18. Y. Liu, M. O’Keeffe, M. M. J. Treacy, O. M. Yaghi, The geometry of periodic knots, polycatenanes and weaving from a chemical perspective: A library for reticular chemistry. *Chem. Soc. Rev.* **47**, 4642–4664 (2018).
19. S. C. Power, I. A. Baburin, D. M. Proserpio, Isotopy classes for 3-periodic net embeddings. *Acta Crystallogr. A Found Adv.* **A76**, 275–301 (2020).
20. A. Holden, *Orderly Tangles: Cloverleafs, Gordian Knots, and Regular Polylinks* (Columbia University Press, New York, 1983).
21. B. Grünbaum, G. Shephard, Symmetry groups of knots. *Math. Mag.* **58**, 161–165 (1985).
22. M. O’Keeffe, M. M. Treacy, Isogonal weavings on the sphere: Knots, links, polycatenanes. *Acta Crystallogr. A Found. Adv.* **76**, 611–621 (2020).
23. J. H. Conway, H. Burgiel, C. Goodman-Strauss, *The Symmetries of Things* (AK Peters Ltd., Wellesley, MA, 2016).
24. S. T. Hyde, S. J. Ramsden, V. Robins, Unification and classification of two-dimensional crystalline patterns using orbifolds. *Acta Crystallogr. A Found. Adv.* **70**, 319–337 (2014).
25. E. Schulte, Chiral polyhedra in ordinary space, I. *Discrete Comput. Geom.* **32**, 55–99 (2004).
26. T. Castle, M. E. Evans, S. T. Hyde, All toroidal embeddings of polyhedral graphs in 3-space are chiral. *New J. Chem.* **33**, 2107–2113 (2009).
27. S. Barthel, On chirality of toroidal embeddings of polyhedral graphs. *J. Knot Theory Ramif.* **26**, 1750050 (2017).
28. T. Castle, “Entangled graphs of surfaces in space,” PhD thesis, Australian National University, Canberra, Australia
29. S. T. Hyde, C. Oguey, From 2D hyperbolic forests to 3D Euclidean entangled thicketts. *Eur. Phys. J. B* **16**, 613–630 (2000).
30. C. Q. Zhang, *Circuit Double Cover of Graphs* (London Mathematical Society Lecture Note Series, Cambridge University Press, Cambridge, UK, 2012), vol. 399.
31. B. Farb, D. Margalit, *A Primer on Mapping Class Groups* (Princeton University Press, Princeton, NJ, 2011).
32. P. R. Cromwell, *Polyhedra* (Cambridge University Press, Cambridge, UK, 1999).
33. P. Pierański, S. Przybył, A. Stasiak, Tight open knots. *Eur. Phys. J. E* **6**, 123–128 (2001).
34. J. Cantarella, R. B. Kusner, J. M. Sullivan, On the minimum ropelength of knots and links. *Invent. Math.* **150**, 257–286 (2002).
35. M. E. Evans, V. Robins, S. T. Hyde, Ideal geometry of periodic entanglements. *Proc. R. Soc. Math. Phys. Eng. Sci.* **471**, 20150254 (2015).
36. E. Flapan, *When Topology Meets Chemistry: A Topological Look at Molecular Chirality* (Cambridge University Press, Cambridge, UK, 2000).
37. H. Moriuchi, A table of handcuff graphs with up to seven crossings. *OCAMI Stud* **1**, 179–200 (2007).
38. C. Liang, K. Mislow, Topological chirality and achirality of links. *J. Math. Chem.* **18**, 1–24 (1995).
39. H. S. M. Coxeter, *Regular Polytopes* (Courier Corporation, North Chelmsford, MA, 1973).
40. D. J. Tranchemontagne, Z. Ni, M. O’Keeffe, O. M. Yaghi, Reticular chemistry of metal-organic polyhedra. *Angew. Chem. Int. Ed. Engl.* **47**, 5136–5147 (2008).
41. M. Li, D. Li, M. O’Keeffe, O. M. Yaghi, Topological analysis of metal-organic frameworks with polytopic linkers and/or multiple building units and the minimal transitivity principle. *Chem. Rev.* **114**, 1343–1370 (2014).
42. W. Klee, Crystallographic nets and their quotient graphs. *Cryst. Res. Technol. J. Exp. Ind. Crystallogr* **39**, 959–968 (2004).
43. A. Fotin *et al.*, Molecular model for a complete clathrin lattice from electron cryomicroscopy. *Nature* **432**, 573–579 (2004).
44. L. Zhang *et al.*, Stereoselective synthesis of a composite knot with nine crossings. *Nat. Chem.* **10**, 1083–1088 (2018).